Neurite-Specific Ca^{2+} Dynamics Underlying Sound Processing in an Auditory Interneurone

T. Baden, B. Hedwig

Department of Zoology, University of Cambridge, Cambridge, United Kingdom

Received 19 June 2006; accepted 12 July 2006

ABSTRACT: **Concepts on neuronal signal processing and integration at a cellular and subcellular level are driven by recording techniques and model systems available. The cricket CNS with the omega-1-neurone (ON1) provides a model system for auditory pattern recognition and directional processing. Exploiting ON1's planar structure we simultaneously imaged free intracellular Ca^{2+} at both input and output neurites and recorded the membrane potential *in vivo* during acoustic stimulation. In response to a single sound pulse the rate of Ca^{2+} rise followed the onset spike rate of ON1, while the final Ca^{2+} level depended on the mean spike rate. Ca^{2+} rapidly increased in both dendritic and axonal arborizations and only gradually in the axon and the cell body. Ca^{2+} levels were particularly high at the spike-generating zone. Through the activation of a Ca^{2+}-sensitive K^+ current this may exhibit a specific control over the cell's electrical response properties. In all cellular compartments presentation of species-specific calling song caused distinct oscillations of the Ca^{2+} level in the chirp rhythm, but not the faster syllable rhythm. The Ca^{2+}-mediated hyperpolarization of ON1 suppressed background spike activity between chirps, acting as a noise filter. During directional auditory processing, the functional interaction of Ca^{2+}-mediated inhibition and contralateral synaptic inhibition was demonstrated. Upon stimulation with different sound frequencies, the dendrites, but not the axonal arborizations, demonstrated a tonotopic response profile. This mirrored the dominance of the species-specific carrier frequency and resulted in spatial filtering of high frequency auditory inputs.** © 2006 Wiley Periodicals, Inc. J Neurobiol 00: 000–000, 2006

Keywords: **Ca^{2+} signaling; dendritic integration; tonotopicity; Ca^{2+}-dependent K^+ current; omega-1-neurone; Oregon Green BAPTA-1**

INTRODUCTION

Computational power and complexity achieved by nervous systems rely on the synaptic connections between neurones and also upon functional properties within each neurone. The response to synaptic inputs, their effects on the activation of secondary ionic currents, and the generation of a spike code as a function of synaptic current and recent neuronal history are central to intra-neuronal processing and integration (Borst and Egelhaaf, 1992; Single and Borst, 1998; Ogawa et al., 2001, 2002; Destexhe and Marder, 2004; London and Häusser, 2005). Comparatively little however is known about how such responses within and between individual neurites are integrated towards shaping the electrical properties of a neurone *in vivo*. By combining electrophysiology and fast optical imaging we analyzed the spatio-temporal Ca^{2+} activation patterns following acoustic stimulation in the cricket auditory interneurone omega-1-neurone (ON1) where Ca^{2+} is involved in "chemical computation" of sound responses (Sobel and Tank, 1994).

ON1 is a bilaterally paired auditory interneurone located in the prothoracic auditory neuropil with well

This article contains supplementary material available via the Internet at http://www.interscience.wiley.com/jpages/0022-3034/suppmat

Correspondence to: T. Baden (tb283@cam.ac.uk).

Contract grant sponsors: Cambridge University Newton Trust, Royal Society, BBSRC, Cambridge European Trust, Department of Zoology Balfour Fund.

Published online in Wiley InterScience(www.interscience. wiley.com).
DOI 10.1002/neu.20323

documented morphology (Wohlers and Huber, 1982), response characteristics (Wohlers and Huber, 1978; Wiese and Eilts, 1985), connectivity (Selverston et al., 1985; Horseman and Huber, 1994; Poulet and Hedwig, 2006) and functionality (Wiese and Eilts, 1985; Pollack, 1988; Sobel and Tank, 1994; Nabatiyan et al., 2003). ON1 receives inputs from ipsilateral auditory afferents originating from the ears in the front legs (Imaizumi and Pollack, 2005) and in turn forms inhibitory connections to its contralateral counterpart (Selverston et al., 1985) and the contralateral ascending auditory interneurones AN1 (Horseman and Huber, 1994; Faulkes and Pollack, 2000) and AN2 (Selverston et al., 1985), which transmit auditory information to the brain (Wohlers and Huber, 1982). The recurrent inhibitory network formed by the two ON1 has been implicated in enhancing bilateral auditory contrast supporting auditory orientation and temporal pattern processing (Wiese and Eilts, 1985; Nabatiyan et al., 2003). At high sound intensities, the neurone integrates a broad range of sound frequencies (Schildberger, 1988). ON1 extends its processes in a narrow plane ($<$150 μm; Watson and Hardt, 1996) nearly parallel to the ventral ganglion surface. Therefore, optical imaging of free intracellular Ca^{2+} is possible simultaneously at input and output regions of the cell.

The monitoring of free intracellular Ca^{2+} is interesting, as it is not only a marker of localized activity within a neurone but also carries great functional importance in regulating cellular processes ranging from ionic currents (Sah and Faber, 2002; Faber and Sah, 2003) to gene transcription (West et al., 2001). Following the approach by Sobel and Tank (1994) we have used the advantages of the cricket ON1 neuron to investigate how [Ca^{2+}] changes during acoustic stimulation within individual neurites of ON1 reflect the cell's spatial and temporal integration of synaptic inputs and spike activity underlying sound processing.

EXPERIMENTAL PROCEDURES

Animals

Female crickets (*Gryllus bimaculatus*) with intact ears were selected from the colony kept at the Department of Zoology, University of Cambridge, which is maintained on a 12L:12D light cycle. Prior to dissection animals were cold anesthetized at 4°C for 10–20 min.

Dissection

Animals were placed ventral side up in Plasticine™. Mid- and hind-legs were pinned down while the front legs were fixed with bee's wax to a holder at the tarsus to keep them in walking position. Additionally, the coxa was waxed to the prothoracic segment. A ring of wax was built-up around the sternite and neck of the animal to hold saline (140 m*M* NaCl, 10 m*M* KCl, 4 m*M* $CaCl_2$, 4 m*M* $NaHCO_3$, 6 m*M* NaH_2PO_4) at all times. The gut was removed via an incision in the abdomen that was sealed with wax afterward. The prothoracic ganglion was exposed and a small metal platform with an optic fiber embedded in it was placed underneath. The optic fiber was used for bright field illumination of the ganglion. The cervical connectives were cut. All peripheral nerves were left intact. The prothoracic ganglion was held in position by a small fork placed on the trunks of the cut connectives. To disconnect the auditory input of an ear [Fig. 5(B–D)], the front leg was cut off at the femur. All experiments were performed at room temperature (21–23°C). A total of $\sim$200 crickets were used, of which, 31 yielded the presented data.

Dye Injection

Tips of thick-walled microcapillaries were back-filled with either 400 μ*M* Oregon Green BAPTA-1 (Molecular Probes, Eugene, OR) dissolved in 400 μ*M* KAc or with 2 m*M* Calcium Green5N (Molecular Probes) dissolved in distilled water. Shafts of electrodes were filled with 1*M* KAc. Resistances of microelectrodes varied between 100 and 200 MΩ. Cells were filled with the Ca^{2+} indicator by applying a 1–4 nA hyperpolarizing current for 5–15 min. We could not control the exact concentration of the dye in the cell. Care was taken to use the lowest possible intracellular dye concentration that would yield detectable fluorescence and minimize chelating artifacts. The electrode was removed and the preparation was left for at least 60 min to allow the dye to diffuse throughout the neuron. Because of the relatively high K_d of Calcium Green5N (14 μ*M*), this dye was preferred for experiments where the temporal dynamics of Ca^{2+} were analyzed (see Fig. 1). Oregon Green BAPTA-1 (K_d: 170 n*M*) was superior in terms of diffusion throughout the cell and brightness, and was used to reveal the spatial distribution of Ca^{2+} as well as for simultaneous recordings of Ca^{2+} and membrane potential (Figs. 2–6). Time courses given indicate the most typical examples of responses, measured with Calcium Green5N.

Electrophysiological Recordings

After the staining procedure, thick-walled micropipettes with resistances of 60–120 MΩ filled with 1 *M* KAc were used to intracellularly record either from the main axonal branch or close to the point of convergence of the two dendritic branches (see Fig. 1), where the neurites have the largest diameter. Recordings lasted for up to 2 h. As this second electrode was nonfluorescing, it did not interfere with optical recordings. Physiological signals were recorded using an SEC-10L amplifier (NPI, Tamm, Germany) and digitized at 10 kHz using an AD board (MIO 16E4 National Instruments, Austin, TX) linked to custom built software running under LabView 5.01 (National Instruments). The manipula-

tion of ionic currents *in vivo* is very difficult in the model system at hand, and was so far not attempted.

Optical Recordings

Injected dyes were excited with monochromatic light at 494 nm (10 nm bandwidth) (Optoscan Monochromator CAIRN Research, Faversham, UK). Indicator fluorescence emission in the range of 515–560 μm was detected by a cooled CCD camera (Andor iXon DV887, back illuminated, 90% quantum efficiency with single photon sensitivity at -65°C, 12 bit amplitude resolution) operating at 90 Hz at 128 $\times$ 128 pixel resolution (10.5 ms integration time, with 0.5 ms interframe intervals). This was attached to a Leica DMLFS microscope. For simultaneous electrophysiological and optical recordings a 10$\times$ dry objective (Leica: N.A. 0.25, 19.5 mm working distance) was used to allow space for the electrode. In all other experiments, a 10$\times$ (N.A. 0.3), 20$\times$ (N.A. 0.5), or 40$\times$ (N.A. 0.8) water immersion objective was used. Data was sampled using AQM Advance 6 software (Kinetic Imaging, Andor, Belfast, N. Ireland).

In each ON1 analyzed the following compartments could clearly be distinguished and were defined as separate regions of interest for image analysis: the axon, two major dendritic branches (D1 and D2), two prominent branches with axonal terminals (T1 and T2), and the spike generating zone (SGZ) [Fig. 1(A)]. This was located next to the convergence point of the two main dendrites where the neurite was particularly thick. Electrophysiological recordings at this region showed small spikes riding on large EPSPs, while recordings further along the axon demonstrated large spikes and no/small EPSPs (Selverston 1985, personal observations). In addition, in some preparations it was possible to image the primary neurite and soma as well when located in the same plane as the rest of the neurone.

Single acoustic stimuli (>60 dB sound pressure level (SPL)) led to fluorescence changes of up to 20% and were clearly detectable in single trials of acoustic stimulation (Figs. 3–5). Averaging over several trials was only used when the exact time course of the Ca^{2+} response was to be analyzed, or particularly small changes in Ca^{2+} were to be detected (Figs. 1, 2, and 6). Because of light scattering, we could not specifically resolve the Ca^{2+} signal in individual small diameter secondary and tertiary neurites of ON1. Therefore, all analysis considers primary neurites and the summed activity of adjacent smaller branches [Fig. 1(B,C)].

Acoustic Stimulation

Sound stimuli were generated in CoolEdit 2000 (Syntrillium, Phoenix, US) and presented by a pair of headphone speakers attached to the wide ends of 15 cm conical copper-tubes acting as sound guides. The speakers were aligned at 90° left and right to the animal's length axis. The narrow end of the tubes was placed 2 cm from the opening of the respective auditory spiracle. Intensities of stimuli were calibrated (amplifier Type 2610 with 4133 microphone Bruel and Kjaer, Nærum, Denmark) to an accuracy of $\pm$1 dB SPL (relative to 2×10^{-5} Pa) at the position of the spiracle. Unless stated otherwise, carrier frequency of sound stimuli was 4.8 kHz. Background noise in the room was <45 dB SPL.

Data Analysis

Imaging data was first converted in AQM Advanced 6 to be read by ImageJ 1.33u (US National Institutes of Health). Gray levels over time could be calculated for arbitrary regions of interest. Values given are changes in fluorescence relative to background intensity at that region ($\Delta F/F$). Imaging data was precisely aligned with electrophysiological data in Neurolab (Hedwig and Knepper, 1992) using camera generated TTL pulses, indicating the timing of every frame taken. Further data analysis was performed using MatLab 6.5 (Mathworks, Natick, MA).

RESULTS

Ca^{2+} Dynamics in Different Neurites

We used a 1 s sound pulse (90 dB SPL, 4.8 kHz) to characterize the spatio-temporal Ca^{2+} response profile of the ON1. Acoustic stimulation led to Ca^{2+} increases in all regions, with the axonal terminals (T1 and T2), the medial dendrite (D1), and the putative SGZ, exhibiting greatest amplitude changes, followed by the lateral dendrite (D2) and the axon (see Fig. 1). Within the dendrite and axonal terminals, the rise times of Ca^{2+} transients in response to acoustic stimulation were faster than decay times ($\tau_{rise} = 177$ ms, $\tau_{decay} = 237$ ms, Calcium Green-5N). Generally, T1 and T2 exhibited slightly faster changes than D1 and D2. In experiments where Oregon Green BAPTA-1 was used, Ca^{2+} dynamics were generally slower, because of the greater chelating effect of the dye.

At the SGZ pronounced Ca^{2+} elevations were present despite the lack of any fine neurites in that region. Here, the Ca^{2+} rise and decay times are slower, ($\tau_{rise} =$ 298 ms, $\tau_{decay} = 1265$ ms) [Fig. 1(D)]. Consequently, the Ca^{2+} level was elevated for hundreds of milliseconds longer than at D1 and D2 or T1 and T2. This relates to a prominent spatial change in the Ca^{2+} distribution. During the first 500 ms of the acoustic stimulus, the peak Ca^{2+} transient at D1 started shifting towards the SGZ at a velocity of $\sim$100 μm/s [Fig. 1(E,F), online material 1]. No Ca^{2+} shift occurred at the axonal side of the neuron despite that a similar spatial arrangement exists prior to the main axonal branching site.

After about 5–10 s of repeated stimulation, even the axon and soma showed distinct Ca^{2+} signals. Time courses of Ca^{2+} elevations here varied as a function of distance from T1, T2 and D1, D2 (data not shown), indicating that Ca^{2+} enters the axon and soma by diffusion from T1, T2 and D1, D2 [see also Fig. 4(C)].

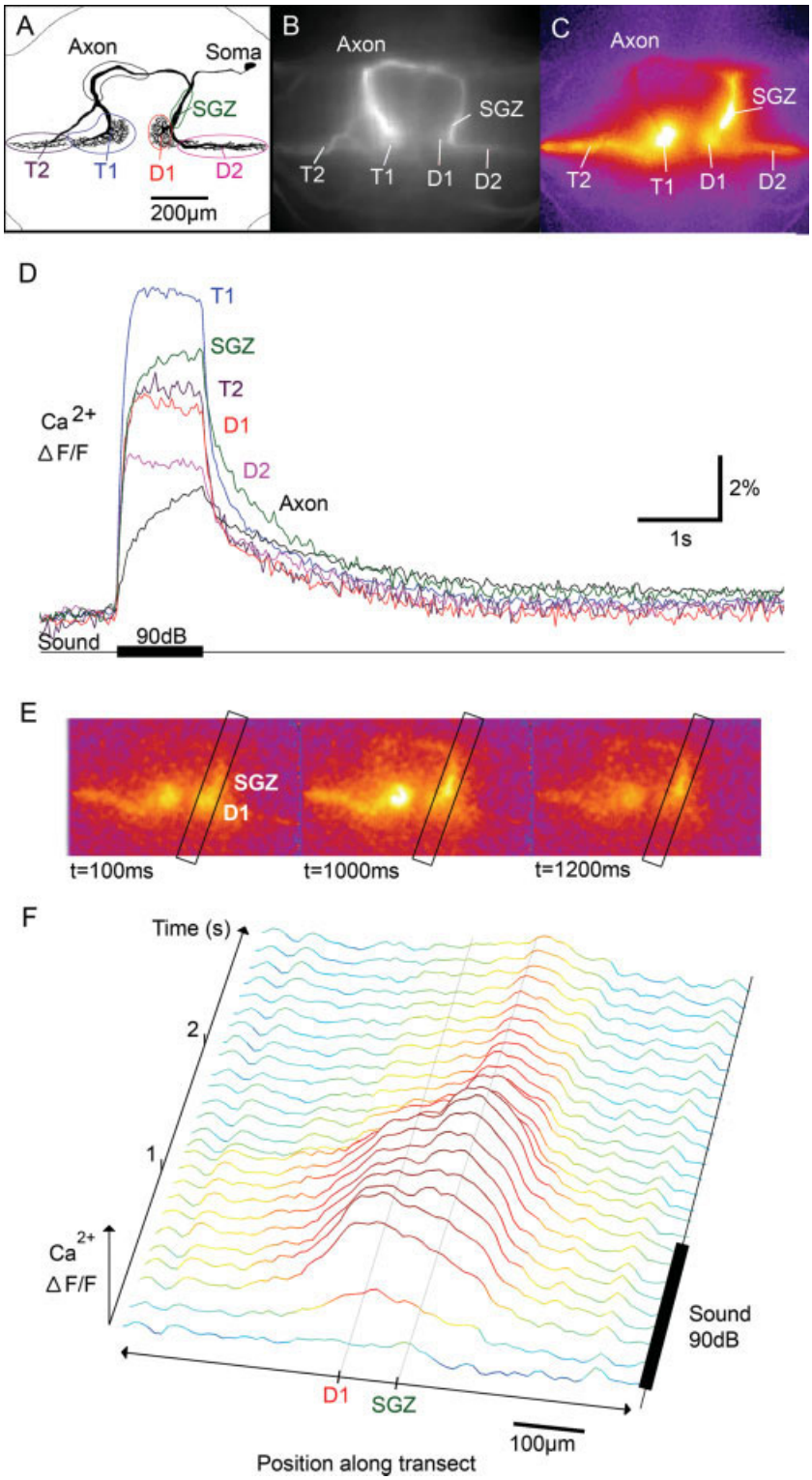
A
Axon
Soma
SGZ
T2
T1
D1
D2
200µm
B
Axon
SGZ
T2
T1
D1
D2
C
Axon
SGZ
T2
T1
D1
D2
D
T1
SGZ
T2
D1
D2
Axon
Ca 2+
ΔF/F
2%
1s
Sound
90dB
E
SGZ
D1
t=100ms
t=1000ms
t=1200ms
F
Time (s)
2
1
Ca 2+
ΔF/F
Sound
90dB
D1
SGZ
100µm
Position along transect

Figure 1

Correlations Between Membrane Potential and Ca^{2+} Dynamics

Upon excitatory synaptic activation, Ca^{2+} may enter the cytosol through voltage or ligand-gated channels as well as through release from intracellular stores (Gallin and Greenberg, 1995; Berridge, 1998). Once inside the cytosol, however, Ca^{2+} may in turn act as a regulator of the cell's excitatory activity through activation of an outward current (Sobel and Tank, 1994; Berridge, 1998; Sah and Faber, 2002). We, therefore, analyzed the relationship between Ca^{2+} and the cell's electrical activity. Since the Ca^{2+} dynamics at D1 and D2 and T1 and T2 respectively were very similar, for further analysis, only T1 *versus* D1 was considered.

We averaged the Ca^{2+} signal triggered by spikes occurring at low discharge rates (<5 Hz) in quiescent preparations. This revealed distinct elevations in Ca^{2+} with a maximum amplitude of $\sim$0.2% change in fluorescence at the SGZ (not shown), the axonal terminals, and the dendrites [Fig. 2(A)]. Following the occurrence of spikes, the Ca^{2+} change exhibited a rapid rising time (<10 ms) followed by a slower decay time (>200 ms).

Since single spikes caused small Ca^{2+} transients, variation of acoustic stimulus parameters should evoke different response patterns in both spike rate and Ca^{2+} transients. Given the putative presence of voltage-gated channels at both T1 and D1, effects on Ca^{2+} transients here may be secondary to effects in spike rate. Increasing ipsilateral sound amplitude from 50 to 90 dB, SPL revealed a linear relationship between stimulus intensity up to 80 dB SPL (note that dB scales logarithmically) and the following four parameters: mean spike rate, peak spike rate, D1 peak Ca^{2+} level, and the reciprocal of the time constant of Ca^{2+} rise ($\tau^{-1}_{Ca^{2+}}$) [Fig. 2(B)]. To separate the effects of peak spike rate and mean spike rate on the Ca^{2+} changes, the onset rate of the sound stimuli was systematically altered. Increasing sound onset rate had a large effect on peak spike rate but only caused a very small decrease of the mean spike rate [Fig. 2(C–E)]. Now, the steady state Ca^{2+} level followed the trend of mean spike rate, while the Ca^{2+} influx rate (proportional to $\tau^{-1}_{Ca^{2+}}$) varied with peak spike rate [Fig. 2(E)].

Once in the cytosol, Ca^{2+} can affect the membrane potential and evoke a hyperpolarization via Ca^{2+} activated K^+ currents (Sobel and Tank, 1994; Sah and Faber, 2002). A pronounced (at least 5 mV) after-hyperpolarization, recorded at T1, followed at the end of acoustic stimulation in ON1 [Fig. 3(A)]. The decay of this hyperpolarization strongly correlated with the decay in Ca^{2+} at the SGZ ($r = -0.9640$), at T1 ($r = -0.9577$) and D1 ($r = -0.9574$) [Fig. 3(B)]. However, within the initial phase when the hyperpolarization is strongest ($\sim$0–1 s after stimulus offset) Ca^{2+} at the SGZ, and to a smaller degree also at T1, is not linearly related to membrane potential, but instead is higher than indicated by the linear regression. This indicates that Ca^{2+} at the SGZ may have a particularly large effect on hyperpolarization.

Since Ca^{2+} entry to ON1 at different compartments occurs over hundreds of milliseconds ($\tau_{rise} = 177$ ms at D1 and $\tau_{rise} = 298$ ms at the SGZ) it probably does not contribute to the rapid decrease of ON1's spike rate after an initial phasic response, which occurs within the first $\sim$50 ms after stimulus onset [Figs. 3(A) and 2(C)], but instead may contribute to a slower component of adaptation.

Figure 1 The spatio-temporal Ca^{2+} profile of the ON1. A: Structure of ON1. Regions highlighted are two main branches of axonal terminals (T1 and T2), two branches of the dendrite (D1 and D2), the SGZ, axon, and soma. B: Oregon Green BAPTA-1 staining of ON1 *in vivo*. All major branches of the neurone can be imaged simultaneously. The soma is out of focus in the top right corner. C: Distribution of Ca^{2+} changes ($\Delta F/F$) after 1 s of acoustic stimulation (90 dB SPL, 4.8 kHz). D: Spatio-temporal Ca^{2+} dynamics ($\Delta F/F$) during acoustic stimulation as in (C), using Calcium Green-5N (10 trials averaged). T1, T2 and D1, D2 exhibited the most pronounced and fastest changes in Ca^{2+} ($\tau_{rise} = 177$ ms, $\tau_{decay} = 237$ ms). Slower, yet similar amplitude changes occurred at the SGZ ($\tau_{rise} = 298$ ms, $\tau_{decay} = 1265$ ms). The axon was slowest to respond, and amplitude and time course varied as a function of distance from D1, D2 and A1, A2 ($\tau_{rise} \gg 500$ ms, $\tau_{decay} \gg 1.5$ s). E: Spatial Ca^{2+} distribution at D1 and SGZ at $t = 100$, 1000, and 1200 ms. Recording as in Figure 1(D). Ca^{2+} entering the cytosol at D1 peaked 100–200 ms after sound pulse onset, and the peak Ca^{2+} transient traveled towards the SGZ during presentation of the acoustic stimulus. After stimulus offset Ca^{2+} remained highest at the SGZ. F: Series of Ca^{2+} $\Delta F/F$ profiles between D1 and the SGZ along transect in (E). Profiles calculated at 100 ms intervals with 10 trials averaged. The peak elevation in Ca^{2+} shifts from D1 towards the SGZ within the first 500 ms of stimulation. At the SGZ, it remained high even seconds after stimulus offset, when Ca^{2+} at D1 had returned to resting levels. Different sets of pseudocolors were used in (E) and (F); ($n = 17$ animals) [See also online material 1].

Temporal Pattern Processing in ON1 and Ca^{2+} Dynamics

How are the changes in Ca^{2+} related to the processing of behaviorally relevant auditory patterns? The calling song of crickets may last for many hours. In *G. bimaculatus* it consists of chirps composed of 4–6 syllables (21 ms duration) at a syllable period approximating 42 ms and a chirp repetition rate around 2 Hz (Doherty, 1985) [Fig. 4(A,B)]. Three time scales are hence to be considered: (1) responses to syllables, (2) responses to chirps, and (3) long-term effects of song processing. During the first 1–2 chirps of calling song presentation, a general Ca^{2+} elevation was established. Ca^{2+} levels oscillated to the chirp pattern of 2 Hz around this elevation [Fig. 4(B)]. After the first 2–3 chirps, oscillations at T1 and D1 were more pronounced (25% of the elevation amplitude) than at the SGZ (15% of the elevation amplitude). At the SGZ this resulted in a greater overall Ca^{2+} elevation to species-specific song than at T1 or D1. Up to natural syllable periods of 42 ms, Ca^{2+} levels did not decay between syllables. With longer syllable periods, a distinct decay in Ca^{2+} between individual syllables occurred [Fig. 4(A)]. The Ca^{2+} dynamics, therefore, exhibited properties of a low pass filter for the syllable pattern.

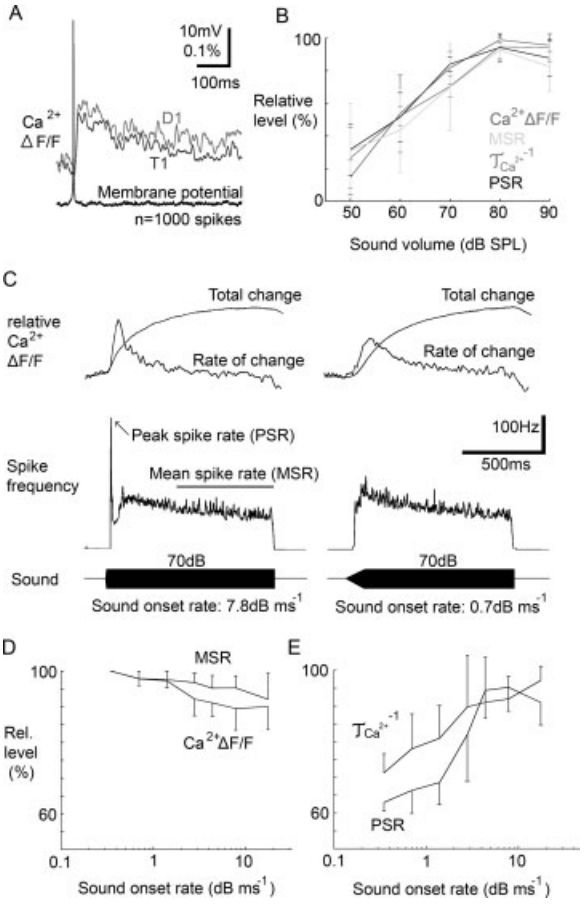

Figure 2 Spike frequency determines Ca^{2+} influx. (A: Average Ca^{2+} responses at T1 and D1 to single spikes generated at low discharge rate (1000 spikes averaged). B: Increasing acoustic stimulus intensity (all 1s 4.8 kHz) from 50 to 90 dB SPL revealed that peak spike rate (PSR), mean spike rate (MSR), final Ca^{2+} level $\Delta F/F$ at D1, and the reciprocal of the time constant of Ca^{2+} rise at D1 ($\tau^{-1}_{Ca^{2+}}$) scale linearly with stimulus intensity up to 80 dB SPL. At 90 dB SPL, the system is saturated. Values were normalized to their maximum (100%). C: Fast sound onset rates resulted in high peak spike rates, independent of mean spike rate. The velocity of Ca^{2+} rise increased for higher peak spike rates. D: Altering sound onset rate only had a small decreasing effect on mean spike rate and D1 final Ca^{2+} level ($\Delta F/F$). E: The sound onset rate had a strong effect on both peak spike rate and the reciprocal of the time constant of Ca^{2+} rise ($\tau^{-1}_{Ca^{2+}}$). Faster onset rates resulted in higher peak spike rates and shorter time constants of Ca^{2+} rise; ($n = 3$ animals).

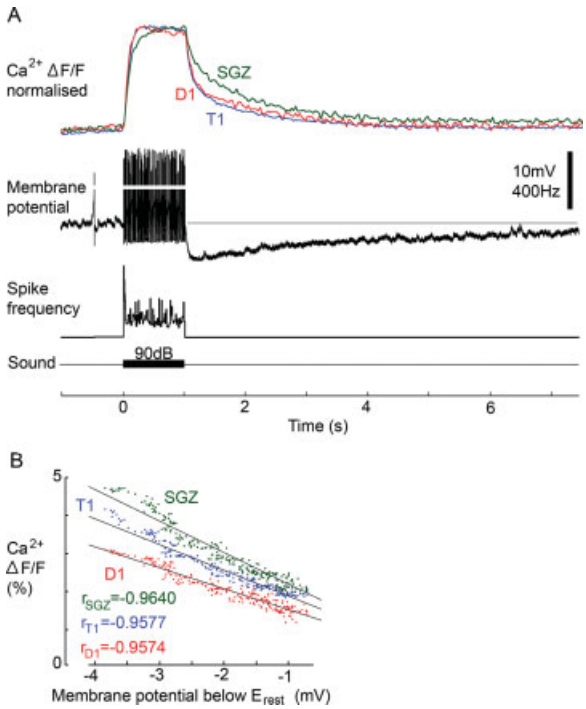

Figure 3 Ca^{2+} Determines membrane potential. A: Single trial of simultaneously recorded responses of membrane potential and Ca^{2+} transients to a 1 s, 90 dB sound pulse. At sound offset, a marked hyperpolarization occurs. Ca^{2+} levels at the SGZ are highest for the entire decay phase. B: The recovery from hyperpolarization strongly correlated with the decay in Ca^{2+} level at the SGZ, D1 and T1; ($n = 3$ animals) [See also online material 1]. [Color figure can be viewed in the online issue, which is available at www.interscience.wiley.com.]

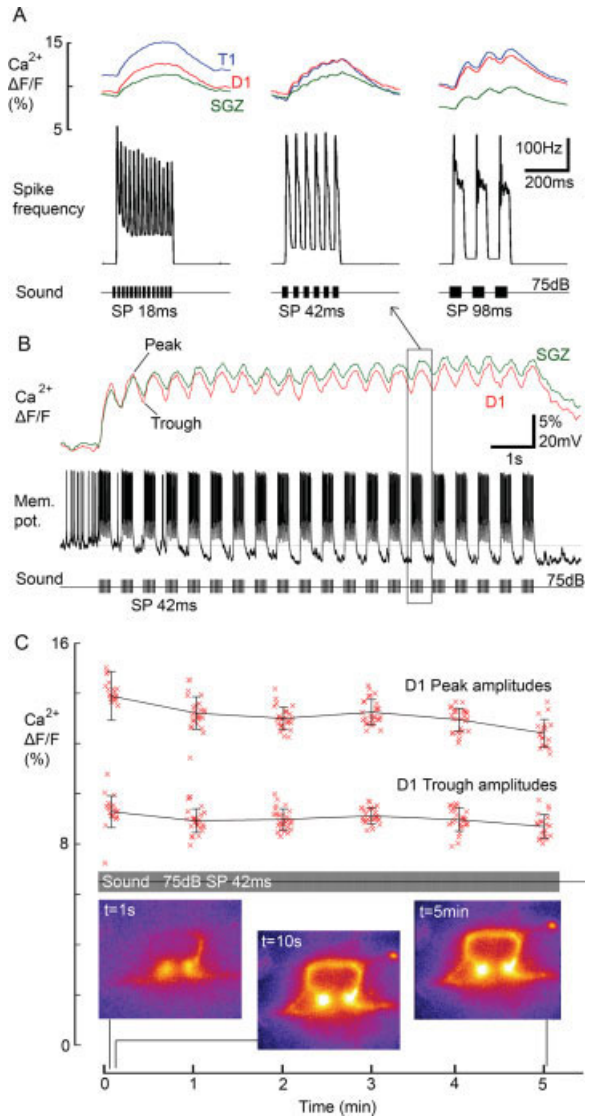

Figure 4 Temporal pattern processing. A: Simultaneously recorded spike frequency and Ca^{2+} dynamics in response to chirps with different syllable periods (SP), averaged over 20 chirps. B: Single trial of spike activity and Ca^{2+} changes in ON1 during presentation of artificial calling song. Ca^{2+} levels increased and clearly oscillated to individual chirps at input regions of the cell (D1), whereas Ca^{2+} at the SGZ showed weaker oscillations. C: Continuous presentation of the artificial calling song for 5 min. Within 10 s of acoustic stimulation, Ca^{2+} transients reached the axon and soma (insets); (A) and (B): $n = 8$ animals with three simultaneous recordings of Ca^{2+} and membrane potential, (C): four animals), [see also online material 2]. [Color figure can be viewed in the online issue, which is available at www.interscience.wiley.com.]

Prolonged stimulation for at least 5 min did not change the oscillation amplitudes and general elevation levels [Fig. 4(C)]. Ca^{2+} signals in axon and soma occurred only after 5–10 s stimulation and then remained high for the duration of extended stimulation.

Integration of Excitatory and Inhibitory Inputs

During phonotaxis, crickets use interaural sound level differences to localize a calling conspecific (Larsen et al., 1989). The paired ON1 enhance bilateral auditory contrast through recurrent inhibition (Selverston et al., 1985; Wiese and Eilts, 1985; Römer and Krusch, 2000). In each ON1, ipsilateral excitation by afferents is processed simultaneously with inhibition from the contralateral ON1. The neuron is therefore a model system for the analysis of the interplay of inhibition with excitation. Low sound amplitudes (60 dB SPL) were used to activate the ears independently. During the ipsilateral presentation of a 2000 ms sound, a second contralateral stimulus of 500 ms duration was given. This led to a sudden cessation in spiking, which then recovered towards a spike rate of 50 Hz while the contralateral stimulus was still on. Simultaneously, a distinct decrease in Ca^{2+} occurred particularly at T1 (28%) and D1 (24%), and to a lesser degree (10%) at the SGZ [Fig. 5(A)].

To dissociate the effects of inhibition and excitation, the ipsilateral ear providing most excitatory auditory inputs (Watson and Hardt, 1996) was removed. Recordings of the membrane potential near T1 now revealed clear IPSPs in response to contralateral acoustic stimulation [Fig. 5(B)]. During contralateral acoustic stimulation, Ca^{2+} decreased by 1% in the dendrite (five out of seven animals, two showed no effect), because of the inhibition suppressing the ongoing spike activity. Ca^{2+} at the axonal branches (T1, T2), however, increased by about 1.5% (about 10 times less than during ipsilateral stimulation) during the inhibition (six out of seven animals) [Fig. 5(C,D)]. This result cannot be explained by the reduced spike activity but rather may indicate a direct synaptic input to the axonal terminals activated by contralateral acoustic stimulation as previously suggested for crickets (Selverston et al., 1985; Watson and Hardt, 1996) as well as bushcrickets (Molina and Stumpner, 2005).

Sound Frequency Integration

The lowest threshold of ON1 is at 4–5 kHz, but it responds to frequencies in a range from 3 to 20 kHz at 75 dB SPL (Schildberger, 1988). Its dendrites extend along the axonal projections of the auditory afferents in the auditory neuropile (Esch and Huber, 1980; Wohlers and Huber, 1982; Imaizumi and Pollack,

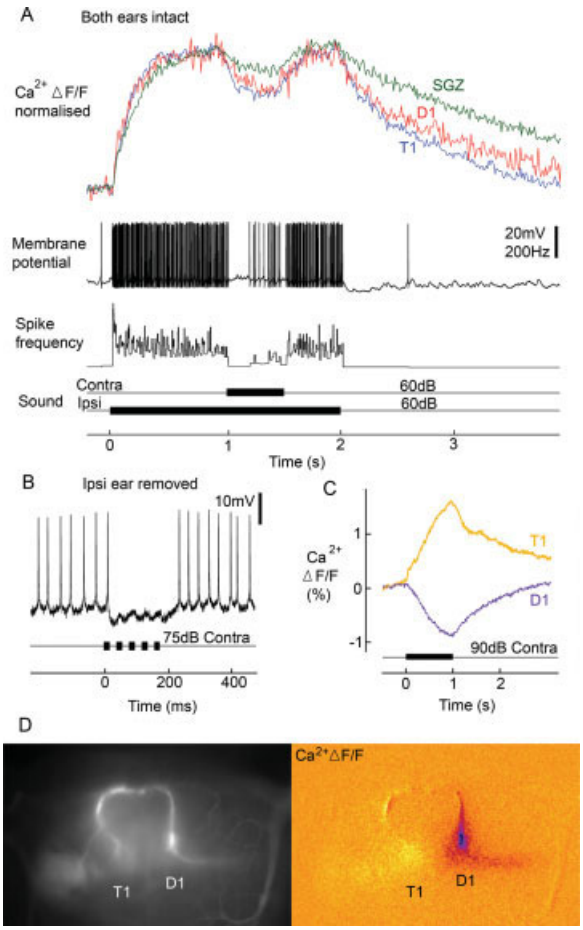

Figure 5 Integration of excitation and inhibition. A: Single trial simultaneous recording of membrane potential and Ca^{2+} dynamics demonstrating contralateral inhibition. Presentation of a short contralateral acoustic stimulus (500 ms, 60 dB SPL) during presentation of a 2000 ms ipsilateral acoustic stimulus (60 dB SPL) resulted in a decreased spike rate. This was accompanied by strong reductions in Ca^{2+} level at D1 and T1, and a weaker reduction at the SGZ. B: After removal of the ipsilateral ear, distinct IPSPs were elicited upon contralateral acoustic stimulation. C: Now, contralateral acoustic stimulation resulted in a decrease of Ca^{2+} at D1, whereas at T1, an increase occurred. D: Spatial distribution of changes as seen in C ($\Delta F/F$) demonstrates the opposite responses in dendrite (D1) and terminals (T1); ((A): $n = 10$ animals, (B-D): 7 animals).

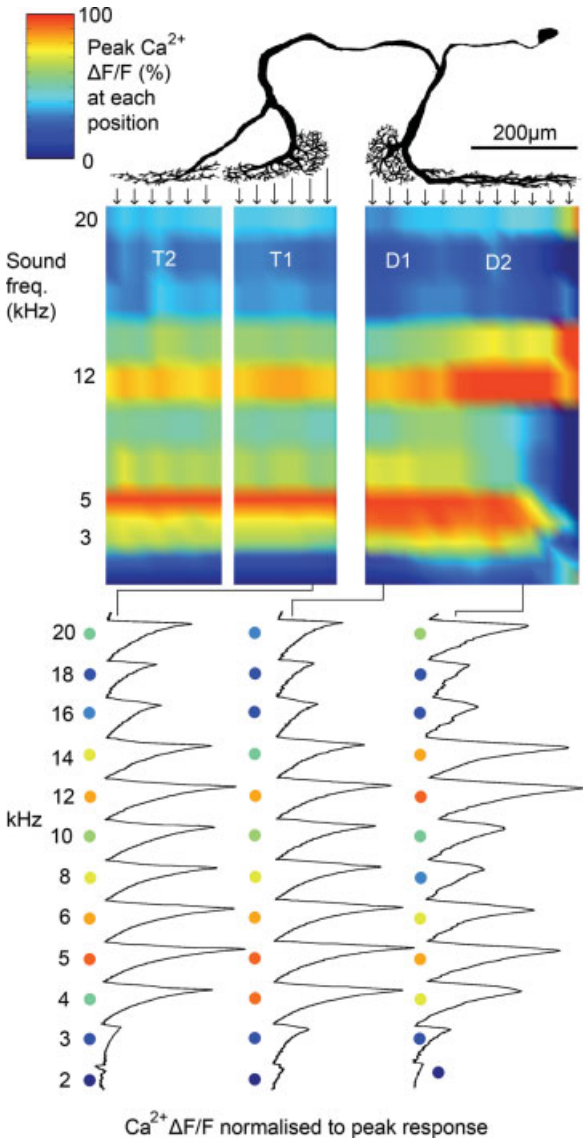

Figure 6 Frequency integration and tonotopicity. Ca^{2+} responses to acoustic stimuli (1 s, 75 dB) at varying sound frequencies, shown for a single anminal. Responses were calculated for adjacent positions along T2, T1, D1, and D2 as indicated by arrows. The responses to all frequencies tested were normalized to the maximal response at each position indicated. Peak Ca^{2+} $\Delta F/F$ to each stimulus are color coded as indicated in the dots next to the example traces. The peaks of the three example traces in the bottom denote the differential frequency tuning at the three positions indicated. A tonotopic organization of inputs along the dendrite (D1 and D2) is revealed. The peripheral dendritic branch (D2) responded strongest to high frequency components (>10 kHz) and D1 responded most strongly to lower frequencies (4–5 kHz). Along the two axonal branches (T1 and T2), no such differentiation occurred ($n = 5$ animals).

2005). We therefore tested for a tonotopic arrangement of auditory inputs along the dendritic branches (D1 and D2). At the axonal terminals (T1 and T2), however, the spatial distribution of Ca^{2+} activity should not depend on input frequency.

ON1 was stimulated with 1 s sounds (75 dB SPL, 0.25 Hz repetition rate) at frequencies between 3 and 20 kHz (steps of 1 kHz for 3–6 kHz, steps of 2 kHz for 8–20 kHz) and Ca^{2+} was imaged. Adjacent

regions of interest were defined along T2, T1, D1, and D2, each covering 35 μm along the length of these neurites (see Fig. 6). The Ca^{2+} response at each region of interest was normalized to the maximum response across the frequencies tested. As expected, along the axonal neurites T1 and T2, which are activated by the spike pattern of the neuron, no spatial pattern of frequency representation occurred. Here, the response to sound frequencies peaked at 4–5 kHz corresponding to the tuning of the neuron (Schildberger, 1988). Along the dendrites D1 and D2, which respond to synaptic potentials and invading spikes, a tonotopic arrangement of sound frequency inputs was observed. The arborizations of D1 responded more strongly to low frequency sound (4–5 kHz), and D2 showed a greater responsiveness to high frequencies ($\sim$12 kHz). The frequency tuning at the axonal terminals (T1 and T2) reflects responses at D1 better than at D2. This is most likely due to the greater spatial proximity of D1 relative to the SGZ. Interestingly, in addition, the low frequency band at T1 and T2 is narrower than at D1 and D2, with responses to frequencies below 4 kHz at T1, T2 being weaker than compared to D1, D2.

DISCUSSION

The planar structure of the ON1 offers the possibility to record Ca^{2+} dynamics in both input and output neurites at the same time, and to relate Ca^{2+} changes to simultaneously recorded electrical activity and the functional properties of the cell.

Methodological Considerations

Because of the nature of our staining and recording techniques it was impossible to determine the absolute concentration of Ca^{2+} dye in the individual compartments of our cells. Inherent to the method, chelating artifacts introduced by the dyes could affect time courses and diffusion velocities measured. For a review of problems associated with Ca^{2+} imaging using fluorescent indicators see Berridge (1998) or Augustine et al. (2003). Several steps were taken to minimize chelating artifacts: (1) minimal concentrations of dye which would yield a detectable fluorescent change upon acoustic stimulation were used. (2) A gap of at least 60 min between the staining and the recording process was left to allow diffusion of the dye throughout the cell. (3) Staining of the cell was performed at two different locations in different experiments (near the SGZ and in the axon near the terminals), and the effects of a dye concentration gradient after 60 min diffusion was judged minimal. (4) A low affinity dye (Calcium Green-5N) was employed to determine more exact time courses (see Fig. 1) and to reduce the extent of chelating artifacts introduced by the higher affinity dye Oregon Green BAPTA-1. Consequently, velocities of Ca^{2+} changes presented in this study are if anything an underestimation, with Fig. 1 presenting the most accurate indication.

The manipulation of specific ionic channels was not attempted. Accordingly, conclusions drawn about possible ionic currents underlying the observed changes in cell physiology in response to acoustic stimulation are based on characterized Ca^{2+} effects in similar studies (Wicher and Penzlin, 1997; Single and Borst, 1998; Nakamura et al., 1999; Augustine et al., 2003).

Ca^{2+} Dynamics in Different Neurites

Ca^{2+} may enter the cytosolic phase in three different ways: (1) entry through voltage-gated Ca^{2+} channels, (2) entry through ligand-gated channels, and (3) release from intracellular stores (Berridge, 1998). Ca^{2+} entry at presynaptic terminals occurs via voltage-gated channels. Ca^{2+} elevations at both the axonal terminals (T1 and T2) and the dendrites (D1 and D2) to single spikes [Fig. 2(A)] suggest the presence of voltage-gated Ca^{2+} channels at both types of neurites, and may underlie the rapid Ca^{2+} dynamics at these branches in response to acoustic stimulation [Fig. 1(D)]. We could not distinguish between contributions from high and low voltage-gated channels (Wicher and Penzlin, 1997). The much slower Ca^{2+} dynamics at soma and axon varied as a function of distance from these primary entry areas and therefore indicates passive diffusion of Ca^{2+} [Fig. 1(A,D)].

Further to voltage-gated channels, a leakage of Ca^{2+} through ligand-gated channels or alternatively its release from intracellular stores at the dendrites (D1 and D2) is suggested by the tonotopic arrangement of excitation. Additionally, the observed small but significant Ca^{2+} elevation in axonal branches upon contralateral acoustic stimulation despite the absence of spike activity indicates an entry of Ca^{2+} through a mechanism other than through voltage-gated channels at the terminals (T1 and T2) [Fig. 6(B–D)]. It can at this point not be concluded whether or not this elevation in Ca^{2+} contributes to the release of synaptic vesicles.

A key question for the function of ON1 is where Ca^{2+} at the SGZ is derived from. The particularly slow Ca^{2+} dynamics at the SGZ are unlikely to be the result of a nonuniform dye distribution as staining ON1 at different sites and with minimum concentrations of

Calcium Green-5N reliably yielded very similar spatio-temporal Ca^{2+} distributions. Instead, they could be a result of the large size of the SGZ. The increased cytoplasmic volume dictates that free intracellular Ca^{2+} concentration rises more slowly than at thinner neurites if the same Ca^{2+} influx occurs. Alternatively, the peak Ca^{2+} transient traveling from D1 to the SGZ [Fig. 1(E,F)] may result from movement of Ca^{2+} ions through the cytosol. In comparison with the similar cytosolic volume compartment at the junction of the axonal terminals (T1) and the axon, the speed and amplitude of Ca^{2+} changes are much greater at the SGZ. A pure passive diffusion model is therefore unsatisfactory, and active transport or propagation processes from the dendrites to the SGZ may have to be assumed. Ca^{2+} waves in neurones of similar spatio-temporal properties have been described previously, e.g. in hippocampal CA1 neurones (Nakamura et al., 1999, 2000).

Interdependence of Ca^{2+} and Membrane Potential

Ca^{2+} enters the cytosolic phase of ON1 as a result of depolarizing synaptic input and/or intracellular release and spike activity. Once inside, Ca^{2+} contributes to the control of the membrane potential, for example through a Ca^{2+} activated K^+ conductance (Sah and Faber, 2002) as in blowfly large monopolar cells (Hardie and Weckström, 1990), cockroach motor neurones (David and Pitman, 1996), lamprey interneurones (El Manira et al., 1994) as well as in ON1 (cricket: *Acheta domestica*, Sobel and Tank, 1994). This negative feedback loop of cell excitability is a key element of ON1 response properties in temporal pattern processing and noise suppression.

We observed that the after-stimulus hyperpolarization correlates with the free cytosolic Ca^{2+} concentration at the SGZ, the dendrites, and the axonal terminals (see Fig. 3). Notably, any dendritic contribution to hyperpolarization will have been attenuated at the recording site near T1. Since the amount of this attenuation is not known it was not included into calculations. Nonetheless, immediately after the end of acoustic stimulation hyperpolarization and Ca^{2+} at the SGZ was particularly high [Figs. 1(D,F) and 3(B)]. This suggests that hyperpolarization of ON1 as a function of its own spike activity may be driven in particular by the SGZ. Functionally, this appears to be a very efficient mechanism of ON1 to control spiking activity. The impact of EPSPs in generating spikes could be reduced at the very site where it is translated into a series of spikes.

Increasing sound intensity resulted in linear increases of the final Ca^{2+} elevation, rate of Ca^{2+} rise, mean spike rate, and peak spike rate relative to the logarithmic dB scale, all saturating at 80 dB [Fig. 2(B)]. Within the range of 50–80 dB, ON1 hence encodes stimulus intensity in dB linearly not only in spike rate parameters but also in Ca^{2+} rate of rise and concentration. Increasing stimulus onset rate strongly increased peak spike rate without changing the final mean spike rate [Fig. 2(C–E)]. Final Ca^{2+} elevation, however, correlated with mean spike rate. This indicates that the peak spike rate does affect the rate of Ca^{2+} rise while the final Ca^{2+} level and the mean spike rate are interdependent. The functional consequence of these particular Ca^{2+} dynamics is that transient peaks in spike rate, thought critical in temporal pattern processing (Nabatiyan et al., 2003), are maintained relative to a generally suppressed background activity. In this way, peaks in spike rate can not only operate to transmit the temporal structure of species-specific song to postsynaptic targets, but at the same time maintain intracellular Ca^{2+} at a high level.

Temporal Pattern Processing

Upon species-specific song presentation Ca^{2+} levels oscillated in the chirp rhythm around a general sustained elevation, the level of which coincides with a simultaneously maintained hyperpolarization between chirps [Fig. 4(B)]. This hyperpolarization has previously been shown to keep background activity below the threshold for spike generation (Pollack, 1988, Sobel and Tank, 1994).

Ca^{2+} did not decay during species-specific intersyllable intervals [Fig. 4(A)]. However, Ca^{2+} levels oscillated in the slower chirp rhythm. Ca^{2+} dynamics in ON1 therefore provide a low pass filter of temporal pattern, as previously shown for peak spike rate (Nabatiyan et al., 2003).

Over prolonged acoustic stimulation, amplitudes of Ca^{2+} oscillations were constant in all cellular compartments [Fig. 4(C)]. Elevations in free intracellular Ca^{2+} occurred only gradually in the axon and the soma, which in insects has only a passive role in electrical signaling. The Ca^{2+} elevation in the cell body may allow an activation of long-term processes such as the mobilization of dormant proteins or even enhanced translation or transcription to meet the requirements of the neurone (West et al., 2001) exposed to continuous song.

Integration of Excitatory and Inhibitory Inputs

The bilaterally paired ON1 form a network of recurrent inhibition (Selverston et al., 1985), which allows for the enhancement of bilateral auditory contrast (Wiese and Eilts, 1985) and supports directional processing.

During sound processing, ON1 integrates ipsilateral excitatory inputs from auditory afferents (Imaizumi and Pollack, 2005) and inhibitory inputs from its contralateral counterpart. Presentation of a contralateral stimulus during ongoing ipsilateral stimulation demonstrated this integration not only in membrane potential but also in the Ca^{2+} signals [Fig. 5(A)]. The initial cessation of spiking in response to the contralateral sound is accompanied by a Ca^{2+} decay rate similar to the Ca^{2+} rate at ipsilateral sound offset. Changes in Ca^{2+} may therefore be the consequence of the decreased spike rate. Again, at the SGZ, the decay in Ca^{2+} due to the inhibition was less pronounced than at the axonal terminals or dendritic areas. Therefore, the two different types of inhibition occurring in ON1, that is external contralateral inhibition and internal Ca^{2+} controlled K^+ conductance at the SGZ, interfere only to a small degree. The functional consequence of this is that in our stimulation paradigm, the two types of inhibition are effectively additive. A decrease in Ca^{2+} due to an inhibitory synaptic input was demonstrated in blowfly tangential neurones (Single and Borst, 1998); however, interactions between excitation and inhibition were not studied in detail.

After removing ipsilateral excitatory inputs, intracellular recordings demonstrated distinct IPSPs to contralateral acoustic stimulation [Fig. 5(B)]. Now, Ca^{2+} at the dendrites (D1 and D2) decreased because of the reduced resting spike activity [Fig. 5(C,D)]. Critically, however, Ca^{2+} at the axonal branches T1 and T2 still showed a clear increase to the contralateral acoustic stimulus. This indicates a contralateral excitatory synaptic input to the axonal terminals of ON1, which was unmasked by removing the ipsilateral ear. It is unclear by what mechanism Ca^{2+} enters ON1 here; however, it is unlikely to be dependent on voltage-gated channels. Presynaptic inputs onto ON1 axonal terminals are indicated on the basis of ultrastructural studies (Watson and Hardt, 1996), and may be the basis for the observed changes.

Sound Frequency Integration

The population of G*ryllus bimaculatus* auditory afferents encodes a frequency range of 3–20 kHz (Oldfield et al., 1986). In other, closely related species, their axonal terminals project in a tonotopic fashion in the prothoracic auditory neuropile (Römer, 2003; Oldfield et al., 1986; Römer et al., 1988). In crickets, high frequency coding afferents terminate both medially and laterally, while lower frequency afferents project medially (Imaizumi and Pollack, 2005). The *G. bimaculatus* ON1 encodes a wider frequency range than individual afferents (Schildberger, 1988; personal observations), and extends its dendrite along the same projection area as the tonotopicity map of afferent terminals.

Accordingly, Ca^{2+} responses along the dendrites revealed a tonotopic input arrangement: medially, low (4–5 kHz) frequency inputs predominated (D1), the medial end of the lateral branches (D2) received both low and high (10–14 kHz) frequency inputs, and towards the lateral tip of the lateral dendrites (D2), low frequency inputs ceased and 20 kHz inputs occurred (see Fig. 6). At the axonal terminals (T1 and T2), no such tonotopicity was observed. Here, high frequency components, although prominent at the lateral dendrite (D2), were weaker than low frequency components. Notably, intracellular diffusion of Ca^{2+} may have contaminated the measurements, which were taken over 1 s, tonotopicity may therefore be more pronounced than presented here.

The large distance of D2 towards the SGZ, when compared with D1 towards the SGZ, may functionally result in spatial filtering of EPSPs between D2 and the SGZ, giving them a weaker effect on spike generation. This demonstrates how tonotopicity can be exploited for sound frequency filtering within a single neurone. However, most synaptic connections between ON1 and auditory afferents are located towards the distal ends of the smaller neurites along D1 and D2 (Watson and Hardt, 1996); therefore, a large proportion of input attenuation may occur before reaching the main dendritic arms. Additionally, Ca^{2+} transients measured at the lateral dendrite (D2) are generally weaker than at the medial dendrite (D1) [Fig. 1(B)]. Pollack (1994) found that presentation of 30 kHz stimuli to ON1 in *Teleogryllus oceanicus* elicited larger EPSP amplitudes at the SGZ than 5 kHz inputs. However, given the increased flight activity and expanded hearing range towards the ultrasound of *T. oceanicus* relative to *G. bimaculatus*, this finding may reflect an increased importance in high frequency sound processing in this species. This may be revealed using Ca^{2+} imaging in the ON1 of *T. oceanicus*.

Interestingly, the broad frequency band centered around 4–5 kHz at the medial dendrite and the medial end of the lateral dendrite is narrower at the axonal terminals, with components below 4 kHz reduced in amplitude. While it is unclear how such frequency filtering is achieved, it cannot result from the distance between inputs and the SGZ.

Future Experiments

The manipulation of ion channels and internal Ca^{2+} release mechanisms through specific blockers could lead to a more complete understanding of the relationship between synaptic inputs, Ca^{2+} entry, and the

activation of hyperpolarizing outwards currents in ON1. Furthermore, site-specific flash photolysis of caged Ca^{2+}, Ca^{2+} buffers, or inositol-1-4-5-triphosphate should clarify the role of the SGZ in supporting the observed gain control properties of ON1.

We thank David Parker, Steven Rogers, Swidbert Ott, Maja Zoroviç, and Olivier Faivre for critical reading of the manuscript and for very helpful discussions.

REFERENCES

Augustine GJ, Santamaria F, Tanaka K. 2003. Local calcium signalling in neurons. Neuron 40:331–346.

Berridge MJ. 1998. Neuronal Ca^{2+} signalling. Neuron 21: 13–26.

Borst A, Egelhaaf M. 1992. In vivo imaging of Ca^{2+} accumulation in fly interneurons as elicited by visual motion stimulation. Proc Natl Acad Sci USA 89:4139–4143.

David JA, Pitman RM. 1996. Cyclic-AMP regulation of Ca^{2+}-dependent K channels in an insect central neurone. Neurosci Lett 203:151–154.

Destexhe A, Marder E. 2004. Plasticity in single neuron and circuit computations. Nature 431:789–795.

Doherty JA. 1985. Trade-off phenomena in calling song recognition and phonotaxis in the cricket *Gryllus bimaculatus* (Orthoptera, Gryllidae). J Comp Physiol [A] 156:787–801.

El Manira A, Tegner J, Grillner S. 1994. Ca^{2+}-dependent potassium channels play a critical role for burst termination in the locomotor network in lamprey. J Neurophysiol 72:1852–1861.

Esch H, Huber F. 1980. Primary auditory neurons in crickets: Physiology and central projections. J Comp Physiol [A] 137:27–38.

Faber LSE, Sah P. 2003. Ca^{2+}-activated potassium channels: Multiple contributions to neuronal function. Neuroscientist 9:181–194.

Faulkes Z, Pollack GS. 2000. Effects of inhibitory timing on contrast enhancement in auditory circuits in crickets (*Teleogryllus oceanicus*). J Neurophysiol 84:1247–1255.

Gallin WJ, Greenberg ME. 1995. Ca^{2+} regulation of gene expression in neurons: The mode of entry matters. Curr Opin Neurobiol 268:367–374.

Hardie R, Weckström M. 1990. Three classes of potassium channels in large monopolar cells of the blowfly *Calliphora vicina*. J Comp Physiol [A] 167:723–736.

Hedwig B, Knepper M. 1992. NEUROLAB, a comprehensive program for the analysis of neurophysiological and behavioural data. J Neurosci Methods 45:135–148.

Horseman G, Huber F. 1994. Sound localisation in crickets. I. Contralateral inhibition of an ascending interneuron (AN1) in the cricket *Gryllus bimaculatus*. J Comp Physiol [A] 175:389–398.

Imaizumi K, Pollack GS. 2005. Central projections of auditory receptor neurons of crickets. J Comp Neurol 493: 439–447.

Larsen ON, Kleindienst HU, Michelsen A. 1989. Biophysical aspects of sound reception. In: Huber F, Moore TE, Loher W, editors. Cricket Behaviour and Neurobiology. Ithaca, London: Cornell University Press, pp364–390.

London M, Häusser M. 2005. Dendritic computation. Annu Rev Neurosci 8:503–532.

Molina J, Stumpner A. 2005. Effects of pharmacological treatment and photoinactivation on the directional responses of an insect neuron. J Exp Zoolog A Comp Exp Biol 303(12):1085–1103.

Nabatiyan A, Poulet JFA, de Polavieja GG, Hedwig B. 2003. Temporal pattern recognition based on instantaneous spike rate coding in a simple auditory system. J Neurophysiol 90:2484–2493.

Nakamura T, Barbara J-G, Nakamura K, Ross WN. 1999. Synergistic release of Ca^{2+} from IP3-sensitive stores evoked by synaptic activation of mGluRs paired with back propagating action potentials. Neuron 24:727–737.

Nakamura T, Nakamura K, Lasser-Ross N, Barbara J-G, Sandler VM, Ross WN. 2000. Inositol 1,4,5-triphosphate (IP3)-mediated Ca^{2+} release evoked by metabotropic agonists and backpropagating action potentials in hippocampal CA1 pyramidal neurons. J Neurosci 20: 8365–8376.

Ogawa H, Baba Y, Oka K. 2001. Dendritic calcium accumulation regulates wind sensitivity via short-term depression at cercal sensory-to-giant interneuron synapses in the cricket. J Neurobiol 46:301–313.

Ogawa H, Baba Y, Oka K. 2002. Spike-triggered dendritic calcium transients depend on synaptic activity in the cricket giant interneurons. J Neurobiol 50:234–244.

Oldfield BP, Kleindienst HU, Huber F. 1986. Physiology and tonotopic organization of auditory receptors in the cricket *Gryllus bimaculatus*. J Comp Physiol [A] 159: 457–464.

Pollack GS. 1988. Selective attention in an insect auditory neuron. J Neurosci 8:2635–2639.

Pollack GS. 1994. Synaptic inputs to the omega neuron of the cricket *Teleogryllus oceanicus*: Differences in EPSP waveforms evoked by low and high sound frequencies. J Comp Physiol [A] 174:83–89.

Poulet JFA, Hedwig B. 2006. The cellular basis of a corollary discharge. Science 311:518–522.

Römer H. 1983. Tonotopic organization of the auditory neuropile in the bushcricket *Tettigonia viridissima*. Nature 306:60–62.

Römer H, Krusch M. 2000. A gain-control mechanism for processing of chorus sounds in the afferent auditory pathway of the bushcricket *Tettigonia viridissima* (Orthoptera, Tettigoniidae). J Exp Biol 186:181–191.

Römer H, Marquart V, Hardt M. 1988. Organization of a sensory neuropile in the auditory pathway of two groups of orthoptera. J Comp Neurol 275:201–215.

Sah P, Faber LES. 2002. Channels underlying neuronal Ca^{2+}-activated potassium currents. Progr Neurobiol 66: 345–353.

Schildberger K. 1988. Behavioural and neuronal mechanisms of cricket phonotaxis. Experimentia 44:408–415.

Selverston AI, Kleindienst HU, Huber F. 1985. Synaptic connectivity between cricket auditory interneurons as studied by selective photoinactivation. J Neurosci 5: 1283–1292.

Single S, Borst A. 1998. Dendritic integration and its role in computing image velocity. Science 281:1848–1850.

Single S, Borst A. 2002. Different mechanisms of Ca^{2+} entry within different dendritic compartments. J Neurophysiol 87:1616–1624.

Sobel EC, Tank DW. 1994. In vivo Ca^{2+} dynamics in a cricket auditory neuron: An example of chemical computation. Science 263:823–826.

Watson AHD, Hardt M. 1996. Distribution of synapses on two local auditory interneurons, ON1 and ON2, in the prothoracic ganglion of the cricket: Relationships with GABA-immunoreactive neuron. Cell Tissue Res 283: 231–246.

West AE, Chen WG, Dalva MB, Dolmetsch RE, Kornhauser JM, Shaywitz AJ, Takasu MA, et al. 2001. Ca^{2+} regulation of neuronal gene expression. Proc Natl Acad Sci USA 98:11024–11031.

Wicher D, Penzlin H. 1997. Ca^{2+} Currents in central insect neurons: Electrophysiological and pharmacological properties. J Neurophysiol 77:186–199.

Wiese K, Eilts K. 1985. Evidence for matched frequency dependence of bilateral inhibition in the auditory pathway of *Gryllus bimaculatus*. Zool Jb Physiol 89:181–201.

Wohlers DW, Huber F. 1978. Intracellular recording and staining of cricket auditory interneurons (*Gryllus campestris L., Gryllus bimaculatus* De Geer). J Comp Physiol [A] 127:11–28.

Wohlers DW, Huber F. 1982. Processing of sound signals by six types of neurons in the prothoracic ganglion of the cricket, *Gryllus campestris L.* J Comp Physiol [A] 146:161–173.